

# Temperature Dependence of Rutile (TiO<sub>2</sub>) and Geikielite (MgTiO<sub>3</sub>) Structures Determined Using Neutron Powder Diffraction

C.M.B. Henderson<sup>1,2,\*</sup>, K.S. Knight<sup>3</sup> and A.R. Lennie<sup>2</sup>

<sup>1</sup>STFC Daresbury Laboratory, Warrington, WA4 4AD; <sup>2</sup>School of Earth, Atmospheric and Environmental Science, University of Manchester, Manchester M13 9PL and <sup>3</sup>ISIS, STFC Rutherford-Appleton Laboratory, Didcot, Oxford OX11 0QX, UK

**Abstract:** The temperature dependences of the structures of rutile and geikielite are reported up to ~1200°C. While the thermal expansion of the unit cell edges for our rutile agree with published data the (Ti-O) bond expansions show significant differences with the longer (T-O) showing a larger thermal expansion coefficient ( $19.3 \times 10^{-6}$ /degree) than the shorter bond ( $2.6 \times 10^{-6}$ /degree). High-temperature crystallographic data for geikielite are reported for the first time and display interesting differences in the thermal behaviour of the (Ti-O) and (Mg-O) octahedra related to edge- and face-sharing. Thus (O-O) edges of faces shared by (Ti-O) and (Mg-O) octahedra contract, (O-O) edges shared by adjacent (Ti-O) (and Mg-O) octahedra show no significant change, and (O-O) edges of unshared faces between (Ti-O) (and Mg-O) octahedra and adjacent vacant sites expand. Mg-Mg and Ti-Ti distances across shared edges diverge at higher temperatures as (Ti-Ti) increases and (Mg-Mg) does not change.

## 1. INTRODUCTION

Lennie *et al.* [1] have recently determined structural changes occurring in synthetic 'karrooite' (MgTi<sub>2</sub>O<sub>5</sub>) as a function of temperature using powder neutron diffraction with particular emphasis being placed on the effects of Mg-Ti site interchange over the two non-equivalent octahedral sites. One of the three samples (Kar2) used in this experiment contained impurities of rutile (TiO<sub>2</sub>) and geikielite (MgTiO<sub>3</sub>), and full Rietveld analysis provided structural data for all three phases. The Rietveld results showed that the initial mole proportions in the as-synthesized sample were karrooite: rutile + geikielite 0.875: 0.125. Above 1000°C, additional karrooite was formed by reaction of rutile and geikielite giving mole proportions at ~1400°C of 0.975: 0.025 [1]. Above ~1200°C the mixture contained too little rutile and geikielite to provide reliable structural data for these impurity phases.

MgTiO<sub>3</sub> occurs as a rare natural mineral [2] but is better known in materials science because of its widespread use in microwave ceramic capacitors and resistors [3]. Its high temperature structural properties are therefore of interest and in this paper we report on the thermal expansion of unit cell edges and detailed structures of geikielite up to ~1100°C (and of rutile up to ~1200°C). To the best of our knowledge, only room temperature crystallographic structural data for geikielite exist in the literature although high-temperature (and high pressure) Raman spectroscopic data have been used to deduce certain structural relationships [4, 5]. However, high pressure crystallographic data have been determined for this phase [6]. Because our structural data are

determined for relatively small amounts of both rutile and geikielite in the sample mixture and their subsequent decrease between 1000 and 1400°C, all of the structural parameters show higher errors than would be ideal. However, our data for rutile are in generally good agreement with published data and this gives us confidence in the geikielite results presented here. Thus the data presented here provide the ability to consider the controls of both bulk thermal expansion, based on unit cell parameters, and the detailed geometry of polyhedral thermal expansion for two phases with very different inter-octahedral linkages. In addition, the high temperature crystallographic data for geikielite can be used to assess the structural deductions from high-temperature Raman spectroscopy [5].

## 2. STRUCTURES OF RUTILE AND GEIKIELITE

Rutile (TiO<sub>2</sub>) crystallises in the tetragonal space group  $P4_2/mnm$  with two formula units of TiO<sub>2</sub> per unit cell [7]. The structure consists of TiO<sub>6</sub> octahedra sharing two opposite edges with adjacent octahedra to build up chains parallel to *c*. The structure is propagated in the (001) plane by corner sharing between chains. The *c* repeat distance is defined by the distance between Ti atoms in a chain (Fig. 1a) and the only variable parameter is the O<sub>x</sub> coordinate. The structure has two non-equivalent nearest neighbour Ti-O distances with the two longer distances (Ti-O<sub>1b</sub>) oriented perpendicular to the *c* axis; the four shorter Ti-O<sub>1a</sub> bonds lie parallel to <110> planes (Fig. 1a).

Geikielite (MgTiO<sub>3</sub>) belongs to the ilmenite structure type (ATiO<sub>3</sub>, A = Mg, Mn, Fe, Zn) with the rhombohedral space group  $R\bar{3}$  and 6 formula units per unit cell [8] and the characteristics of the structure-type are clearly summarised by Wechsler and Prewitt [9]. The geikielite structure is shown in Fig. (1b,c) with the labelling of O atoms taken

\*Address correspondence to this author at the STFC Daresbury Laboratory, Warrington, WA4 4AD, UK; Tel: 0161 881 1852; E-mail: michael.henderson@manchester.ac.uk

from [6]. Each  $\text{MgO}_6$  octahedron shares a face with a  $\text{TiO}_6$  octahedron to form a dimeric unit (see O1-O2-O3 face in Fig. 1b); the opposite faces of these dimers share 'faces' with vacant octahedral sites (Fig. 1b). Note that along the  $c$  axis the same atom type occurs on each side of a vacant site, in effect defining Mg and Ti octahedral vacancies. Alternating layers of Mg and Ti octahedra occur perpendicular to the  $c$  axis (Fig. 1b) with three dimers defining the  $c$  axis repeat. In the  $xy$  plane each  $\text{TiO}_6$  octahedron shares an edge with three adjacent Ti-octahedra (as do  $\text{MgO}_6$  octahedra) to form 6-rings of octahedra with the centres of adjacent Mg-O<sub>6</sub> and Ti-O<sub>6</sub> rings displaced by  $\frac{1}{2}a-\frac{1}{2}a$  in the rhombohedral  $x$ - $y$  plane (Fig. 1c). Each  $\text{MgO}_6$  octahedron (and each  $\text{TiO}_6$  octahedron) has two different M-O distances, three longer ones directed towards the shared face and three shorter ones towards the opposite, unshared face. Four different length (multiplicity 3) O-O edges occur in each  $\text{MgO}_6$  octahedron [and each  $\text{TiO}_6$  octahedron]: shared edge (O1-O4, [O3-O9]), unshared edge (O1-O6, [O3-O8]), shared face (O1-O2, = [O1-O3]), unshared face (O4-O6, [O8-O9]) (Fig. 1b). The space group requires that the Mg and Ti atoms are fully ordered and neutron powder diffraction on samples quenched from high-temperature [8] and *in situ*, high-temperature Raman scattering [4] have confirmed that no disordering can be detected; note that full disordering would require a phase transition to the corundum space group,  $R\text{-}3c$ .

### 3 MATERIALS AND METHODOLOGY

#### 3.1. Synthesis and Sample Characterisation

Sample Kar2, of bulk composition  $\text{MgTi}_2\text{O}_5$ , was synthesised in air from reagent grade  $\text{MgO}$  and  $\text{TiO}_2$  dried at  $200^\circ\text{C}$ , mixed in stoichiometric proportions, and heated in a Pt crucible at  $1200^\circ\text{C}$  for 48 hours. It was then cooled, re-ground, annealed for a further 72 hours at  $1200^\circ\text{C}$ , then removed from the furnace and allowed to cool in air. Before and after the heating experiments, the sample was characterised by X-ray powder diffraction using a Philips PW1060 X-ray diffractometer fitted with a curved crystal graphite monochromator, and using a  $\text{Cu K}\alpha$  radiation source. Room temperature unit cell parameters were determined using Si as internal standard. In addition, the sample was analysed before the heating experiments using a Cameca SX100 electron microprobe with  $\text{MgO}$  and  $\text{TiO}_2$  as primary standards. The rutile and geikielite analyses were within error of the stoichiometric formulae. For further details see [1].

#### 3.2. Neutron Diffraction

*In situ* high temperature neutron time-of-flight diffraction experiments on the sample were carried out on the POLARIS diffractometer of the ISIS spallation source, Rutherford Appleton Laboratory. POLARIS is a medium resolution, time-of-flight high intensity neutron powder diffractometer which allows studies of materials under non-ambient conditions.

The sample was pressed to form pellets which were stacked as a pile, held in a tantalum wire basket, and suspended inside the RISO furnace, which has tantalum elements allowing temperatures up to  $2000^\circ\text{C}$  to be attained; temperatures were measured with a W/Re thermocouple. The RISO furnace assembly was evacuated to a pressure of  $\sim 5 \times 10^{-4}$  mbar. After the experiments it was found that the

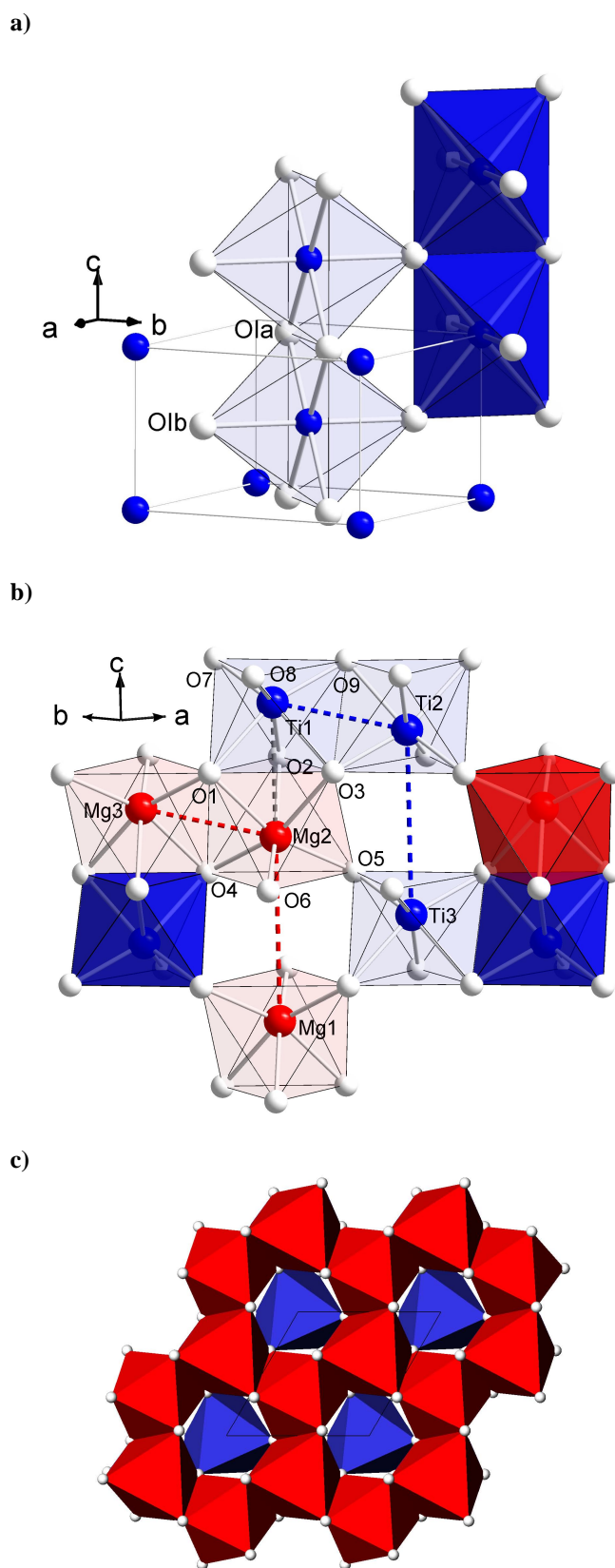


**Fig. (1).** (a) Perspective view of rutile structure with labeled O atoms as white spheres and Ti atoms as blue spheres; (b) Linkage of octahedra for geikielite parallel to the  $\langle 110 \rangle$  plane with O atoms labeled after Yamanaka *et al.* [6]; (c) Linkage of octahedra in geikielite looking down the  $c$  axis.

recorded temperature of ~1600°C is likely to have been 100-150° lower than indicated by the thermocouple. Reliable temperatures were obtained by multiplying the measured temperatures by a correction factor of 0.9329 [1].

Diffraction data were collected only during the heating cycle for about 80 minutes (200 μA) at each temperature with neutron flight times between 2.5 and 19.6 ms, corresponding to *d*-spacings between 0.4 and 3.2 Å in the 2θ = 90° detectors. Data from individual detectors were corrected for electronic noise, normalised against standard spectra from a sample of vanadium, and focused using in-house software. No corrections were made for beam attenuations by the furnace or sample, as they were found to be negligible. The data range included a total of ~3500 independent Bragg reflections for the three phases present.

Analysis of data used full Rietveld refinements in the program GSAS [10] to provide structural information. The background signal was modelled using a 6th-order Chebyshev polynomial. The crystallographic variables were the unit-cell parameters, coordinates of O, Mg and Ti atoms, and isotropic temperature factors. Further information on the experimental approach is given in [1].

Equations used for calculating O-O distances and M-M distances in geikielite are given below where the atom numbering is as shown in Fig. (1b) (O numbering after [6]).

#### O-O Distances in Mg Octahedra

Shared edge between adjacent Mg octahedra:

$$O1-O4 = \{ [a^2 \{ (\frac{1}{3}-2x)^2 + (\frac{1}{3}-2x)(\frac{1}{3}+2y) + (\frac{1}{3}+2y)^2 \} + c^2 (\frac{2}{3}-2z)^2 ] \}^{1/2}$$

Unshared edge:

$$O1-O6 = \{ [a^2 \{ (\frac{1}{3}+y-x)^2 - (\frac{1}{3}+y-x)(\frac{2}{3}-x) + (\frac{2}{3}-x)^2 \} + c^2 (\frac{2}{3}-2z)^2 ] \}^{1/2}$$

Edge at shared face between Mg and Ti octahedra:

$$O1-O2 = a \{ [(-2x+y)^2 - (-2x+y)(-x-y) + (-x-y)^2] \}^{1/2}$$

Edge at unshared face (next to vacant Mg octahedron):

$$O4-O6 = a \{ [(x+y)^2 - (x+y)(1-x+2y) + (1-x+2y)^2] \}^{1/2}$$

#### O-O Distances in Ti Octahedra

Shared edge between adjacent Ti octahedra:

$$O3-O9 = \{ [a^2 \{ (\frac{1}{3}-2y)^2 - (\frac{1}{3}-2y)(-\frac{1}{3}+2x-2y) + (-\frac{1}{3}+2x-2y)^2 \} + c^2 (-\frac{1}{3}+2z)^2 ] \}^{1/2}$$

Unshared edge:

$$O3-O8 = \{ [a^2 \{ (\frac{2}{3}-x+y)^2 - (\frac{2}{3}-x+y)(\frac{1}{3}-x) + (\frac{1}{3}-x)^2 \} + c^2 (\frac{1}{3}-2z)^2 ] \}^{1/2}$$

Edge at shared face between Mg and Ti octahedra:

$$O3-O1 = a \{ [(-x-y)^2 - (-x-y)(x-2y) + (x-2y)^2] \}^{1/2}$$

Edge at unshared face (next to vacant Ti octahedron):

$$O8-O9 = a \{ [(1-x-y)^2 - (1-x-y)(x-2y) + (x-2y)^2] \}^{1/2}$$

#### Metal-Metal Distances

Distance through vacant Mg octahedron:

$$Mg1-Mg2 = c(1-2z_{Mg})$$

Distance through shared edge between adjacent Mg-octahedra:

$$Mg2-Mg3 = \frac{1}{3}([3a^2 + c^2(1-3z_{Mg})^2])$$

Distance through shared edge between adjacent Ti-octahedra:

$$Ti1-Ti2 = \frac{1}{3}([3a^2 + c^2(1-6z_{Ti})^2])^{1/2}$$

Distance through vacant Ti octahedron:

$$Ti2-Ti3 = c(2z_{Ti})$$

Distance through shared face between Mg- and Ti-octahedra:

$$Mg2-T1 = c(z_{Mg}-z_{Ti})$$

We also used the program IVTON [11] to calculate MO<sub>6</sub> polyhedral volumes from geikielite and rutile unit cell and atomic positional parameters. Bond angle variance and mean bond lengths of these polyhedra were calculated from the listing of bond angles and distances output from GSAS. The mean octahedron bond lengths are calculated from the six metal - anion bond lengths of each octahedron

$$\left( \sum_{i=1}^6 M - O_i \right) / 6,$$

and the quadratic elongation (QE) from

$$\left( \sum_{i=1}^6 (l_i / l_o)^2 \right) / 6,$$

where *l<sub>i</sub>* is each individual octahedral bond length and *l<sub>o</sub>* is the centre-to-vertex length for a regular octahedron having the same volume as the distorted octahedron [12]. Bond angle variance (BAV) is calculated using the twelve O-M-O angles defined by taking adjacent anions and measuring the bond angle (θ) through the central cation of each polyhedron

$$\left( \sum_{i=1}^{12} (\theta_i - 90)^2 \right) / 11 [12].$$

## 4. RESULTS AND DISCUSSION

### 4.1. Room Temperature Structural Properties

The room temperature unit cell parameters and other data for our samples of rutile and geikielite can be compared with published values for these minerals in Table 1 and show excellent agreement. However, the O<sub>x</sub> atomic coordinate for our sample of rutile is larger than literature values leading to slightly shorter Ti-O<sub>1a</sub>, longer Ti-O<sub>1b</sub> and shorter O<sub>1a</sub>-O<sub>1a</sub> (shared) bond lengths for our sample (Table 1). These differences lead to our values for the quadratic elongation (1.011) and bond angle variance (36.9) of the TiO<sub>6</sub> polyhedron being slightly larger than those reported by Meagher and Lager [13] (1.008 and 28.7°, respectively).

The atomic coordinates for our sample of geikielite at room temperature can be compared with published values [6, 8, 21] in Table 1. Calculated room temperature Mg-O, Ti-O, Mg-Mg, Mg-Ti, Ti-Ti bond lengths, bond angles, and distortion parameters for our geikielite are given in Table 2 where they can be compared with published values for geikielite and for isostructural ilmenite (FeTiO<sub>3</sub> [9]). The published

**Table 1. Structural Parameters of Rutile and Geikielite at Room Temperature**

Rutile	a, Å	c, Å	V, Å <sup>3</sup>	O <sub>x</sub>	Ti-O1a, Å	Ti-O1b, Å	O1a-O1a Shared, Å	O1a-O1a Unshared, Å
This work	4.5923(3)	2.9576(3)	62.37	0.3092(6)	1.930(3)	2.008(4)	2.479(7)	2.958(7)
Meagher & Lager [13]	4.593(2)	2.959(2)	62.42	0.3051(7)	1.947(2)	1.982(3)	2.532(5)	2.959(2)
Burdett <i>et al.</i> [14]	4.59308(4)	2.95889(3)	62.422	0.30476(6)	1.9486(3)	1.9796(4)	2.536(1)	2.979(1)
Sugiyama & Takeuchi [15]	4.5924(2)	2.9575(2)	62.38(1)	0.30499(8)	1.947	1.981	2.533(1)	2.957(1)
Seki <i>et al.</i> [16]	4.5934	2.9575	62.40					
Abrahams & Bernstein [17]	4.59366(2)	2.95868(1)	62.433	0.3051(2)	1.9485(5)	1.9800(9)	2.536(2)	2.959(2)
Rao <i>et al.</i> [18]	4.5941	2.9589	62.45					
Merz <i>et al.</i> [19]	4.5937	2.9593	62.45					
Taylor [20]	4.5929	2.9591	62.38					
Geikielite	a, Å	c, Å	V, Å <sup>3</sup>	Mg <sub>z</sub>	Ti <sub>z</sub>	O <sub>x</sub>	O <sub>y</sub>	O <sub>z</sub>
This work	5.0543(4)	13.896(2)	307.4(1)	0.352(1)	0.147(2)	0.321(2)	0.025(1)	0.2435(5)
Wechsler & Von Dreele [8]	5.05478(26)	13.8992(7)	307.56(4)	0.35570(5)	0.14510(7)	0.31591(8)	0.02146(8)	0.24635(3)
Yamanaka <i>et al.</i> [6]	5.0540(9)	13.898(1)	307.4(1)	0.35563(6)	0.14496(2)	0.3159(1)	0.0218(1)	0.24641(6)
Liferovich & Mitchell [21]	5.0567(1)	13.9034(2)	307.88(1)	0.3599(1)	0.1459(1)	0.3192(5)	0.0214(7)	0.2458(2)

data for geikielite show significant differences but our data show rather larger differences for some parameters (e.g., Mg-O, Ti-O, and Mg-Ti distances) compared to the literature values. Thus the octahedral volume for MgO<sub>6</sub> in our sample is larger and the TiO<sub>6</sub> volume smaller than published values. In addition, the bond angle variance for TiO<sub>6</sub> is larger than that for MgO<sub>6</sub> which is opposite to the relationship found by other authors for MgTiO<sub>3</sub> and for geikielite structures in general [21-23]. Note that the bond angle variance for TiO<sub>6</sub> in geikielite is significantly larger than that in rutile which is presumably related to the larger number of shared edges in the former (three shared edges plus one shared face) compared to the latter (two shared edges).

#### 4.2. Structural Changes with Increasing Temperature

Cell parameters and atomic coordinates as a function of temperature for rutile and geikielite are given in Table 3. The O<sub>x</sub> coordinate for rutile shows a small increase with increasing temperature although Meagher and Lager [13] did not detect any change. In contrast, none of the atomic coordinates for geikielite are precise enough to show any clear dependence on temperature so we cannot comment on any change in the ‘puckering’ of the layers in the *xy* plane discussed by Wechsler and Prewitt [9] for ilmenite as a function of temperature and pressure, and by Liferoich and Mitchell [21-23] for a series of geikielite analogues containing various M<sup>2+</sup> cations at room temperature and pressure.

Variation of unit cell parameters with temperature for rutile are displayed in Fig. (2) and those for geikielite in Fig. (3); all parameters show linear trends within error. The unit cell linear thermal expansion coefficients are summarised in

Table 4 where our data for rutile can be seen to show excellent agreement with published values (also see Fig. 2).

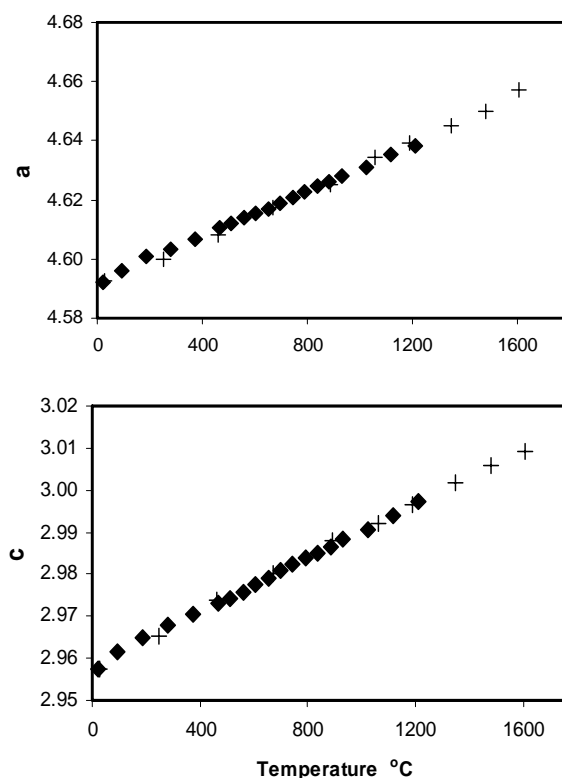


**Fig. (2).** Temperature dependence of unit cell edges for rutile: solid diamonds are our data and plus signs are data from Sugiyama & Takéuchi [15].

Table 2. Room Temperature Structural Data for Geikielite (MgTiO<sub>3</sub>) and Ilmenite (FeTiO<sub>3</sub>)

	This Work	Yamanaka <i>et al.</i> [6]	Liferovich & Mitchell [21]	Wechsler & von Dreele [8]	Wechsler & Prewitt [9]
	Mg-O <sub>6</sub>				Fe-O <sub>6</sub>
M-O1 (sh face) x3	2.154(13)	2.1655(9)	2.177(3)	2.168(1)	2.2013(8)
M-O4 (unsh face) x3	2.082(9)	2.0480(8)	1.998(3)	2.047(1)	2.0778(8)
<M-O>	2.118(16)	2.1067(12)	2.088(5)	2.108(7)	2.1396(12)
O1-O4 (sh edge)	3.068	2.9442(9)	2.916	2.979	3.051(1)
O1-O6 (unsh edge)	2.998	2.9781(9)	2.903	2.947	3.005(1)
O1-O2 (sh face)	2.709	2.6750(6)	2.711	2.677	2.701(1)
O4-O6 (unsh face)	3.194	3.1878(7)	3.135	3.185	3.216(1)
^O4-M-O6 (unsh face)	100.2(5)	102.21(9)	103.34	102.15	101.40(3)
^O1-M-O2 (sh face)	77.9(5)	76.31(7)	77.02	76.25	75.68(3)
Oct vol Mg-O <sub>6</sub>	12.30	11.99(1)	11.64	11.993	12.562
QE	1.020	1.027(1)	1.030	1.0274	1.0271
BAV	69.3	94.0(3)	96.2	92.5	91.8
	Ti-O <sub>6</sub>				
Ti-O1 (sh face)	2.076(18)	2.0912(7)	2.122(3)	2.090(1)	2.0886(8)
Ti-O7 (unsh face)	1.850(14)	1.8658(5)	1.888(3)	1.867(1)	1.8744(8)
<Ti-O>	1.963(23)	1.9785(9)	2.005(5)	1.979(12)	1.9815(12)
O3-O9 (sh edge)	2.538	2.6134(9)	2.695	2.615	2.607(1)
O3-O8 (unsh edge)	2.822	2.8810(9)	2.907	2.879	2.885(1)
O1-O3 (sh face)	2.709	2.6750(7)	2.711	2.677	2.701(1)
O8-O9 (unsh face)	2.873	2.9140(7)	2.927	2.916	2.921(1)
^O8-Ti-O9 (unsh face)	101.9(9)	102.69(3)	101.64	102.69	102.35(3)
^O1-Ti-O3 (sh face)	81.4(8)	79.52(3)	79.42	79.65	75.68(3)
Oct vol Ti-O <sub>6</sub>	9.759	9.926(9)	10.39	9.934	10.001
QE	1.026	1.030(1)	1.026	1.0295	1.0277
BAV	79.6	54.0(7)	78.6	91.2	86.0
M1-Ti1	2.847	2.9318(4)	2.946	2.927	2.9435(4)
M1-M2	2.963	2.9854(4)	2.994	2.984	3.0027(1)
Ti1-Ti2	2.969	2.9809(3)	2.978	2.979	2.9928(1)

The temperature dependence of bond lengths, bond angles, octahedral volumes and distortion parameters for rutile are given in Table 5. Table 4 also shows thermal expansion coefficients for Ti-O<sub>1a</sub> and Ti-O<sub>1b</sub> bonds in our rutile compared with published values. Although the published values show considerable differences between different studies, our data show much greater differences characterised by a smaller expansion coefficient for Ti-O<sub>1a</sub> and a larger one for Ti-O<sub>1b</sub>; this is well shown in Fig. (4) where our data are compared with those of Sugiyama and Takéuchi [15]. The

variations of the different O-O bond distances with increasing temperature (Fig. 5), compared with those from [15], show overlapping trends for O<sub>1a</sub>-O<sub>1a</sub> (unshared) and O<sub>1a</sub>-O<sub>1b</sub> defining small expansions. However, note that our value for O<sub>1a</sub>-O<sub>1a</sub> (shared) is slightly smaller than the published values and our data might even show a very small contraction (Fig. 5). This real decrease parallels the 'relative' shortening of O<sub>1a</sub>-O<sub>1a</sub> (shared) reported by Sugiyama and Takéuchi [15]. Note that this contraction is matched by a trend of decreasing O<sub>1a</sub>-Ti-O<sub>1a</sub> angles (shared) with increasing temperature

**Table 3. Cell Parameters and Atomic Coordinates for Rutile and Geikielite (1 Standard Error in Brackets) Versus Temperature**

°C	a, Å	c, Å	V, Å <sup>3</sup>	O <sub>x</sub>	a, Å	c, Å	V, Å <sup>3</sup>	Mg <sub>z</sub>	Ti <sub>z</sub>	O <sub>x</sub>	O <sub>y</sub>	O <sub>z</sub>
	Rutile				Geikielite							
23	4.5922(3)	2.9576(3)	62.371(9)	0.3092(6)	5.0543(4)	13.896(2)	307.40(6)	0.3519(10)	0.1470(18)	0.3214(22)	0.0254(15)	0.2435(5)
93	4.5961(3)	2.9616(3)	62.561(9)	0.3091(6)	5.0594(4)	13.914(2)	308.44(6)	0.3511(11)	0.1465(18)	0.3242(25)	0.0267(16)	0.2453(5)
186	4.6007(3)	2.9648(3)	62.753(9)	0.3104(7)	5.0644(4)	13.934(2)	309.49(6)	0.3509(12)	0.1478(20)	0.3237(27)	0.0272(18)	0.2451(5)
280	4.6034(3)	2.9678(3)	62.893(9)	0.3100(7)	5.0687(4)	13.949(2)	310.35(6)	0.3514(12)	0.1485(19)	0.3226(27)	0.0266(18)	0.2449(5)
373	4.6068(3)	2.9704(3)	63.042(9)	0.3101(7)	5.0732(4)	13.962(2)	311.18(6)	0.3513(13)	0.1494(21)	0.3227(28)	0.0261(19)	0.2457(5)
466	4.61051(3)	2.9731(3)	63.199(10)	0.3109(7)	5.0774(4)	13.980(2)	312.11(6)	0.3505(16)	0.1475(20)	0.3204(28)	0.0265(20)	0.2456(6)
513	4.6119(3)	2.9743(3)	63.262(9)	0.3112(7)	5.0801(4)	13.988(2)	312.61(6)	0.3495(15)	0.1481(18)	0.3236(29)	0.0274(19)	0.2460(6)
559	4.6141(3)	2.9758(3)	63.355(9)	0.3099(7)	5.0833(4)	13.995(2)	313.17(6)	0.3471(19)	0.1453(18)	0.3233(31)	0.0275(20)	0.2455(7)
606	4.6154(3)	2.9777(4)	63.431(10)	0.3110(8)	5.0848(4)	14.006(2)	313.61(6)	0.3473(23)	0.1452(18)	0.3205(31)	0.0256(22)	0.2456(7)
653	4.6170(3)	2.9790(4)	63.502(10)	0.3100(8)	5.0875(4)	14.013(2)	314.10(6)	0.3518(19)	0.1472(21)	0.3210(33)	0.0249(23)	0.2449(7)
699	4.6189(3)	2.9810(4)	63.599(10)	0.3110(8)	5.0897(4)	14.028(2)	314.69(6)	0.3501(20)	0.1466(21)	0.3214(32)	0.0261(22)	0.2453(7)
746	4.6206(3)	2.9824(4)	63.675(10)	0.3115(8)	5.0926(4)	14.035(2)	315.21(6)	0.3490(20)	0.1475(20)	0.3218(32)	0.0270(22)	0.2456(7)
792	4.6227(4)	2.9839(4)	63.763(10)	0.3119(8)	5.0955(4)	14.041(2)	315.71(6)	0.3509(22)	0.1453(22)	0.3190(31)	0.0256(23)	0.2454(8)
839	4.6247(4)	2.9852(4)	63.846(11)	0.3125(8)	5.0983(4)	14.051(2)	316.29(6)	0.3470(24)	0.1453(20)	0.3189(29)	0.0277(22)	0.2457(8)
886	4.6262(4)	2.9864(4)	63.915(11)	0.3120(8)	5.1015(4)	14.058(2)	316.83(7)	0.3492(23)	0.1460(22)	0.3168(30)	0.0255(23)	0.2450(7)
932	4.6280(4)	2.9882(4)	64.001(11)	0.3116(8)	5.1032(4)	14.071(2)	317.33(7)	0.3496(25)	0.1446(21)	0.3200(33)	0.0263(24)	0.2461(9)
1026	4.6309(4)	2.9907(4)	64.137(12)	0.3126(9)	5.1089(5)	14.090(3)	318.48(7)	0.3473(28)	0.1452(21)	0.3154(30)	0.0253(25)	0.2451(8)
1119	4.6355(4)	2.9938(4)	64.330(13)	0.3128(10)	5.1143(5)	14.108(3)	319.57(8)	0.3515(34)	0.1447(31)	0.3134(33)	0.0240(28)	0.2439(9)
1212	4.6382(6)	2.9973(6)	64.479(17)	0.3137(13)	5.1208(7)	14.129(4)	320.86(11)	0.3450(60)	0.1415(34)	0.3140(40)	0.0280(40)	0.2445(14)
1305	4.6403(15)	3.0003(15)	64.603(46)	0.3137(20)	5.135(3)	14.105(17)	322.13(46)	0.3446(70)	0.1415(60)	0.3142(46)	0.0278(50)	0.2445(24)

**Table 4. Thermal Expansion Coefficients (Units 10<sup>-6</sup>/Degree) for Unit Cell Parameters and T-O Bondlengths for Rutile and Geikielite (this work) and Published Data for Rutile**

	$\alpha_a$	$\alpha_c$	$\alpha_v$	$\alpha_{\text{Ti-O1a}}$	$\alpha_{\text{Ti-O1b}}$	$\alpha_{\text{Mg-O1a}}$	$\alpha_{\text{Mg-O1b}}$
<b>Rutile</b>							
This work	8.25	10.86	27.35	2.36	19.3		
Meagher & Lager [13]	7.4	10.4	25.2	8.7	7.4		
Burdett <i>et al.</i> [14]				4.9	5.7		
Sugiyama & Takeuchi [15]	8.9	11.1	28.9	8.4(3)	11.5(3)		
Seki <i>et al.</i> [16]	8.64	11.63	28.9				
Rao <i>et al.</i> [18]	7.25	8.82	23.3				
Merz <i>et al.</i> [19]	8.34	10.77	27.5				
Taylor [20]	7.61	9.87	25.1				
<b>Geikielite</b>				$\alpha_{\text{Ti-O1}}$	$\alpha_{\text{Ti-O7}}$	$\alpha_{\text{Mg-O1}}$	$\alpha_{\text{Mg-O4}}$
This work	10.6	13.6	34.8	10.90	12.7	-8.2	26.0

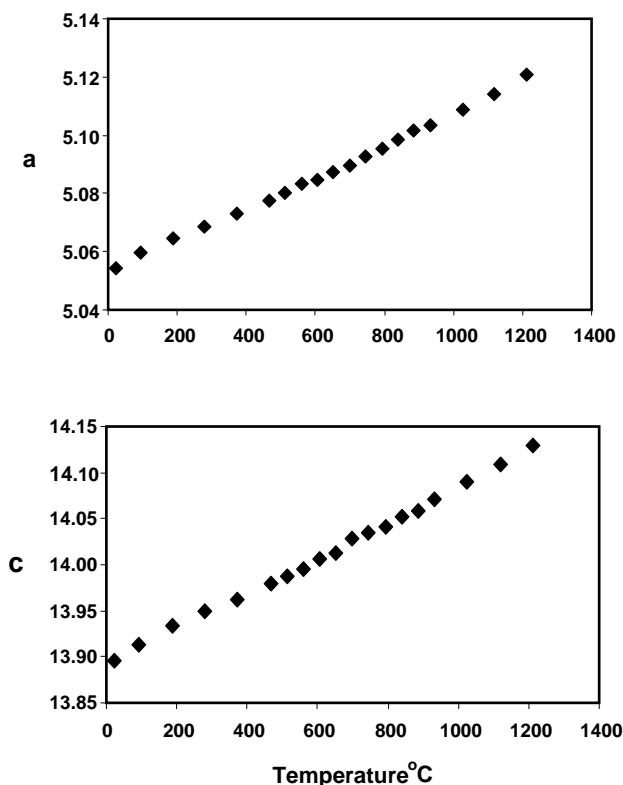


Fig. (3). Temperature dependence of unit cell edges for geikielite.

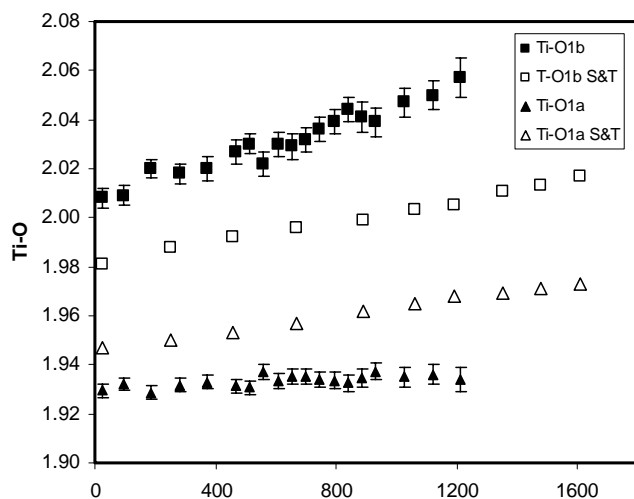


Fig. (4). Variation of Ti-O distances with temperature for rutile (error bars are  $\pm 1\sigma$ ). Solid symbols from this work, open symbols are for data from Sugiyama & Takéuchi [15].

(Table 5) and could reflect an increased repulsion between adjacent Ti atoms as thermal motion increases with increasing temperature [15]. As expected, the octahedral volume, quadratic elongation and bond angle variance of the Ti-O<sub>6</sub> polyhedron for rutile all show clear thermal increases despite the relatively large experimental errors (Table 5).

Although the absolute values for our structural data for both rutile and geikielite are likely to be less reliable than the published data for single-phase samples we believe that the trends with temperature will provide useful information, in

particular for geikielite, where our work is the first to address the high temperature crystallographic properties of this mineral.

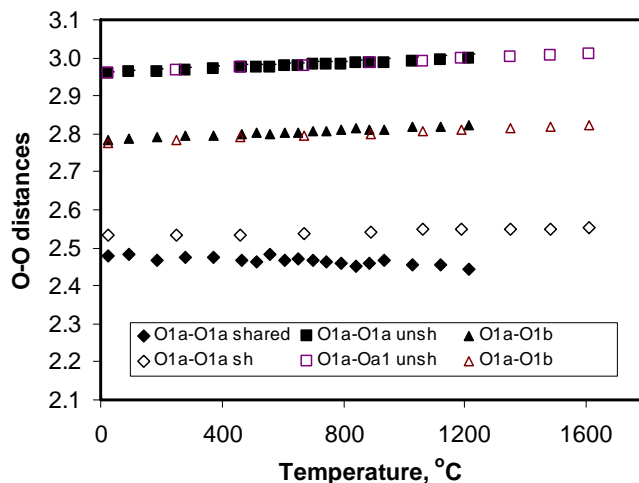


Fig. (5). Variation of O-O distances with temperature for rutile (error bars are  $\pm 1\sigma$ ). Solid symbols from this work, open symbols are for data from Sugiyama & Takéuchi [15]. Note that the O<sub>1a</sub>-O<sub>1a</sub> is the shared edge between octahedra oriented along the *c* axis.

The temperature dependence of bond distances, angles and octahedral distortion parameters for geikielite are given in Table 6. At low temperature the Mg-O1 (shared face) bond length is larger than Mg-O4 (unshared face) but the former stays fairly constant while Mg-O4 shows a small increase, so that by  $\sim 900^\circ\text{C}$  they are not significantly different (Fig. 6). In contrast, the TiO<sub>6</sub> octahedron is more elongate with the Ti-O1 (shared face) being only slightly smaller than the Mg-O1 bond length and the Ti-O7 (unshared face) bond length being much smaller (Fig. 6). Both the Ti-O bond lengths show small expansions with temperature with the shorter Ti-O bond showing the larger expansion. This is the opposite relationship to that deduced for the TiO<sub>6</sub> polyhedron in geikielite by Okada *et al.* [5] and our data are in line with the shorter Si-O and Ge-O bonds in ilmenite-type MgSiO<sub>3</sub> and MgGeO<sub>3</sub> [5] showing larger thermal expansions than the longer Si-O and Ge-O bonds. For the MgO<sub>6</sub> octahedron, O4-O6 (unshared face) shows a small increase, O1-O2 (shared

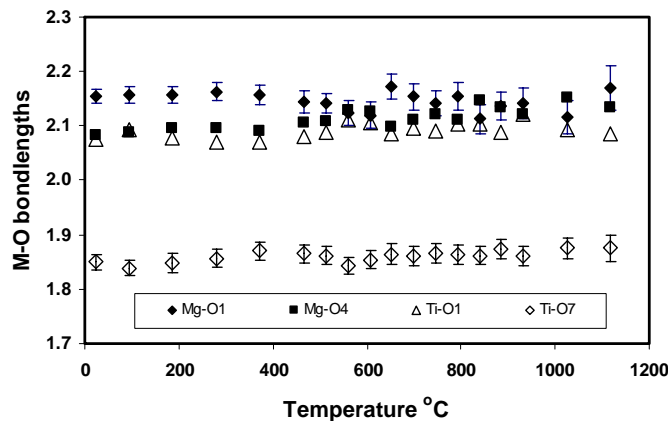


Fig. (6). Variation of M-O distances with temperature for geikielite (error bars are  $\pm 1\sigma$ ). Note that Mg-O1 and Ti-O1 are distances to the shared face between TiO<sub>6</sub> and MgO<sub>6</sub> octahedra.

Table 5. Temperature Dependence of Rutile Bond Lengths, Bond Angles, Ti-O<sub>6</sub> Octahedral Volumes and Distortion Parameters

°C	T-T Å	Ti-O <sub>1a</sub> Å	Ti-O <sub>1b</sub> Å	<Ti-O> Å	O <sub>1a</sub> -O <sub>1a</sub> (s) Å	O <sub>1a</sub> -O <sub>1b</sub> Å	O <sub>1a</sub> -O <sub>1a</sub> (u) Å	<O-O> Å	O <sub>1a</sub> -Ti-O <sub>1a</sub> (s) deg	Ti-O <sub>1a</sub> -Ti deg	V <sub>oct</sub> Å <sup>3</sup>	QE(Ti)	BAV deg <sup>2</sup>
Multiplicity		4	2		2	8	2		2 [+ 2 x (180 - O <sub>1a</sub> -T-O <sub>1a</sub> )]				
23	2.9576(3)	1.9295(3)	2.008(4)	1.9557	2.479(7)	2.785(7)	2.958(7)	2.763	79.93(18)	129.97(9)	9.813	1.0112	36.87
93	2.9616(3)	1.9321(3)	2.009(4)	1.9577	2.482(7)	2.787(7)	2.962(7)	2.765	79.93(19)	129.97(9)	9.844	1.0112	36.87
186	2.9648(3)	1.9285(3)	2.020(4)	1.9590	2.467(7)	2.793(7)	2.965(7)	2.767	79.53(20)	129.77(10)	9.849	1.0123	39.86
280	2.9678(3)	1.9318(3)	2.018(4)	1.9605	2.474(7)	2.794(7)	2.968(7)	2.769	79.62(20)	129.81(10)	9.878	1.0118	39.18
373	2.9704(3)	1.9330(3)	2.020(5)	1.9620	2.474(8)	2.796(8)	2.970(8)	2.771	79.59(21)	129.79(10)	9.900	1.0119	39.41
466	2.9731(3)	1.9313(3)	2.027(5)	1.9632	2.466(8)	2.800(9)	2.973(8)	2.773	79.34(22)	129.67(11)	9.908	1.0127	41.32
513	2.9743(3)	1.9309(3)	2.030(4)	1.9639	2.463(7)	2.802(7)	2.974(7)	2.774	79.26(20)	129.63(10)	9.912	1.0132	41.94
559	2.9758(3)	1.9372(3)	2.022(5)	1.9655	2.481(8)	2.800(8)	2.976(8)	2.776	79.64(21)	129.82(11)	9.953	1.0118	39.03
606	2.9777(4)	1.9336(3)	2.030(5)	1.9657	2.468(8)	2.904(9)	2.978(8)	2.777	79.30(23)	129.65(11)	9.942	1.0129	41.63
653	2.9790(4)	1.9354(3)	2.029(5)	1.9666	2.472(8)	2.804(9)	2.979(8)	2.778	79.37(22)	129.68(11)	9.960	1.0126	41.09
699	2.9810(4)	1.9352(3)	2.032(5)	1.9675	2.469(8)	2.806(9)	2.981(8)	2.779	79.26(23)	129.63(12)	9.969	1.0129	41.94
746	2.9824(4)	1.9339(3)	2.036(5)	1.9679	2.463(8)	2.808(9)	2.982(8)	2.780	79.10(23)	129.55(12)	9.970	1.0134	43.20
792	2.9839(4)	1.9336(3)	2.039(5)	1.9687	2.460(9)	2.810(9)	2.984(9)	2.781	79.01(24)	129.50(12)	9.976	1.0138	43.92
839	2.9851(4)	1.9326(3)	2.044(5)	1.9697	2.453(9)	2.813(9)	2.987(9)	2.782	78.80(24)	129.40(12)	9.976	1.0149	45.61
886	2.9864(4)	1.9347(4)	2.041(6)	1.9701	2.460(9)	2.812(10)	2.986(9)	2.783	78.97(25)	129.48(13)	9.997	1.0139	44.24
932	2.9882(4)	1.9374(4)	2.039(6)	1.9713	2.467(9)	2.813(10)	2.988(9)	2.784	79.08(25)	129.54(13)	10.019	1.0135	43.36
1026	2.9907(4)	1.9350(4)	2.047(6)	1.9723	2.455(10)	2.817(11)	2.991(10)	2.786	78.76(26)	129.38(13)	10.017	1.0149	45.94
1119	2.9938(4)	1.9360(4)	2.050(6)	1.9740	2.455(11)	2.820(11)	2.994(11)	2.788	78.70(30)	129.35(15)	10.045	1.0147	46.43
1212	2.9972(6)	1.9340(5)	2.057(8)	1.9750	2.445(13)	2.823(14)	2.997(12)	2.789	78.40(35)	129.20(19)	10.049	1.0156	48.93
1305	3.0003(6)	1.9354(6)	2.058(7)	1.9764	2.446(14)	2.825(15)	3.000(15)	2.791	78.371(35)	129.19(17)	10.068	1.0157	49.18

face with TiO<sub>6</sub>) a poorly defined small decrease, and O1-O6 (unshared edge) and O1-O4 (shared edge with MgO<sub>6</sub>) exhibit no significant change (Fig. 7). For the TiO<sub>6</sub> octahedron, O3-O9 (shared edge with TiO<sub>6</sub>), O3-O8 (unshared edge) and O8-O9 (unshared face) show small increases and O3-O1 (shared face with MgO<sub>6</sub>) a decrease with increasing temperature (Fig. 7, Table 6). It seems that the O-O edges of the unshared faces for both MgO<sub>6</sub> and TiO<sub>6</sub> octahedra are less constrained and are therefore able to expand slightly with increasing temperature. In contrast, the O-O shared edges show no significant change and the O-O edges of the shared faces appear to contract. Thus, more-complex inter-octahedral linkages within the polyhedral network appear to lead to restricted and variable thermal expansion effects for the geikielite structure. While the distortion parameters (both QE and BAV) are similar for MgO<sub>6</sub> and TiO<sub>6</sub> at low temperatures, at higher temperatures the distortion of TiO<sub>6</sub> increases while that for MgO<sub>6</sub> shows no significant change (Table 6).

Although the Mg-Mg and Ti-Ti distances are subject to considerable errors some interesting relationships can be identified (Table 6). The Mg-Mg and Ti-Ti distances across

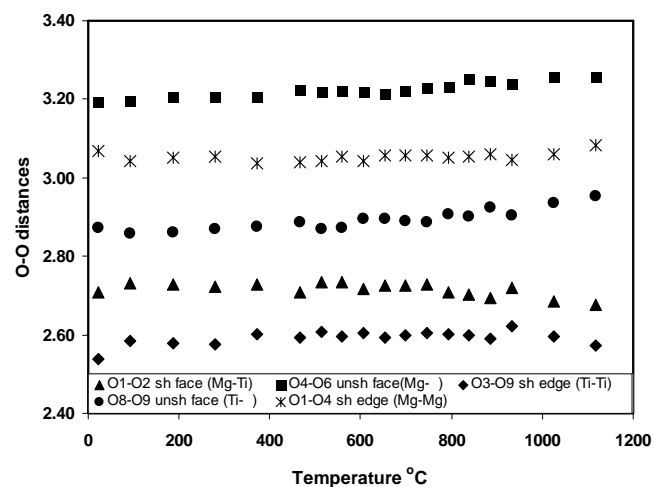


Fig. (7). Variation of O-O distances with temperature for geikielite (error bars are  $\pm 1\sigma$ ). Note that O1-O2 distances are for the shared face between TiO<sub>6</sub> and MgO<sub>6</sub> octahedra.

**Table 6. Temperature Dependence of Structural Parameters in Geikielite**

°C	Mg-O <sub>6</sub>											Mg-Mg	Mg-Ti	Mg-Mg
	Mg-O1	Mg-O4	O1-O2	O1-O4	O1-O6	O4-O6	^O1-Mg-O2 Shared Face	^O4-Mg-O6 Unsh Face	Oct vol	QE	BAV			
23	2.154(13)	2.082(9)	2.7093	3.068	2.9979	3.194	77.9(5)	100.2(5)	12.30	1.020	69.3	2.963	2.847	4.116
93	2.157(15)	2.088(10)	2.7316	3.042	2.9539	3.196	78.6(5)	99.8(5)	12.42	1.018	63.1	2.962	2.847	4.144
186	2.157(16)	2.097(11)	2.7280	3.051	2.9626	3.206	78.4(6)	99.7(5)	12.49	1.018	63.9	2.964	2.830	4.155
280	2.163(16)	2.096(11)	2.7229	3.054	2.9727	3.208	78.0(6)	99.9(5)	12.52	1.019	67.3	2.969	2.830	4.146
373	2.157(17)	2.091(12)	2.7281	3.037	2.9573	3.206	78.4(7)	100.1(6)	12.43	1.019	65.8	2.971	2.819	4.152
466	2.144(20)	2.106(14)	2.7087	3.040	2.9664	3.223	78.3(8)	99.9(7)	12.45	1.018	65.1	2.970	2.838	4.180
513	2.142(18)	2.108(13)	2.7348	3.043	2.9523	3.218	79.3(8)	99.5(7)	12.49	1.016	57.5	2.967	2.817	4.210
559	2.124(22)	2.130(16)	2.7335	3.055	2.9659	3.222	80.1(10)	98.3(8)	12.58	1.013	47.1	2.960	2.824	4.280
606	2.119(24)	2.126(18)	2.7170	3.042	2.9725	3.219	79.7(11)	98.4(9)	12.50	1.014	49.2	2.961	2.831	4.278
653	2.172(23)	2.098(16)	2.7255	3.058	2.9902	3.212	77.7(9)	99.9(8)	12.61	1.020	68.9	2.982	2.867	4.154
699	2.154(24)	2.112(16)	2.7256	3.057	2.9814	3.222	78.5(10)	99.4(9)	12.61	1.018	61.2	2.976	2.855	4.206
746	2.142(23)	2.122(16)	2.7272	3.056	2.9742	3.230	79.1(10)	99.1(8)	12.61	1.016	56.3	2.973	2.828	4.239
792	2.154(26)	2.112(18)	2.7095	3.051	2.9867	3.233	77.9(11)	99.9(9)	12.58	1.019	67.5	2.983	2.887	4.187
839	2.113(27)	2.146(19)	2.7021	3.054	2.9794	3.254	79.5(12)	98.6(10)	12.60	1.014	51.3	2.969	2.836	4.297
886	2.137(26)	2.133(18)	2.6937	3.059	3.0033	3.246	78.2(11)	99.1(9)	12.64	1.017	61.3	2.979	2.857	4.240
932	2.142(28)	2.120(20)	2.7197	3.045	2.9736	3.239	78.8(12)	99.6(10)	12.58	1.017	60.4	2.981	2.884	4.232
1026	2.116(30)	2.152(22)	2.6860	3.060	3.0097	3.256	78.8(14)	98.3(12)	12.67	1.015	53.7	2.976	2.848	4.303

°C	Ti-O <sub>6</sub>											Ti-Ti	Ti-Ti
	Ti-O1	Ti-O7	O3-O9	O3-O8	O1-O3	O8-O9	^O8-Ti-O9 Unshared Face	^O1-Ti-O3 Shared Face	Oct vol	QE	BAV		
23	2.076(18)	1.850(14)	2.538	2.822	2.709	2.873	101.9(9)	81.9(4)	9.759	1.0256	79.7	2.969	4.085
93	2.092(18)	1.839(15)	2.583	2.863	2.732	2.857	101.9(9)	81.9(4)	9.794	1.0266	79.0	2.974	4.077
186	2.078(20)	1.848(17)	2.578	2.865	2.728	2.861	101.4(10)	81.8(5)	9.779	1.0243	74.6	2.971	4.119
280	2.069(20)	1.857(16)	2.577	2.863	2.723	2.871	101.2(10)	81.9(5)	9.783	1.0235	71.6	2.970	4.143
373	2.071(21)	1.870(17)	2.601	2.881	2.728	2.875	100.4(11)	82.4(5)	9.927	1.0210	64.9	2.968	4.172
466	2.080(21)	1.865(17)	2.594	2.887	2.709	2.887	101.5(11)	82.0(6)	9.897	1.0255	78.3	2.980	4.124
513	2.089(20)	1.862(16)	2.608	2.895	2.735	2.869	100.8(9)	82.3(5)	9.983	1.0231	70.7	2.978	4.143
559	2.111(20)	1.843(16)	2.596	2.887	2.733	2.872	102.4(9)	81.8(6)	9.930	1.0296	87.2	2.995	4.067
606	2.107(21)	1.854(17)	2.604	2.889	2.717	2.894	102.6(10)	81.9(6)	9.974	1.0297	90.0	2.996	4.067
653	2.086(23)	1.864(19)	2.593	2.872	2.726	2.896	102.0(11)	81.9(6)	9.930	1.0260	79.0	2.987	4.126
699	2.096(22)	1.860(18)	2.599	2.886	2.726	2.891	101.0(11)	81.9(6)	9.968	1.0269	75.8	2.992	4.113
746	2.091(22)	1.866(18)	2.604	2.897	2.727	2.887	101.4(11)	82.1(6)	10.000	1.0249	76.8	2.989	4.140
792	2.103(23)	1.863(18)	2.602	2.894	2.709	2.908	102.6(12)	81.8(7)	9.992	1.0306	91.2	3.002	4.080
839	2.103(22)	1.862(17)	2.599	2.909	2.702	2.903	102.5(11)	81.7(6)	9.981	1.0309	94.0	3.004	4.083
886	2.087(23)	1.873(18)	2.591	2.892	2.694	2.923	102.6(12)	81.5(7)	9.947	1.0298	91.9	3.002	4.105
932	2.122(24)	1.861(18)	2.622	2.915	2.720	2.905	102.6(12)	82.0(7)	10.126	1.0309	93.6	3.011	4.069
1026	2.094(22)	1.875(18)	2.597	2.902	2.686	2.936	103.0(11)	81.5(7)	9.997	1.0312	97.9	3.011	4.092

the shared edges in the  $xy$  plane are very similar at lower temperatures (Fig. 8) but diverge at higher temperature as the Ti-Ti distance expands while Mg-Mg does not change significantly. In contrast, the Mg-Mg and Ti-Ti distances across the vacant octahedral sites (parallel to  $z$ ) show the opposite effects with Mg-Mg expanding to larger values than the Ti-Ti distances which exhibit no significant change with increasing temperature (Table 6, Fig. 9). Note, however, that the Mg-Ti distances across the shared face are too scattered to identify any trend with temperature (Fig. 8).

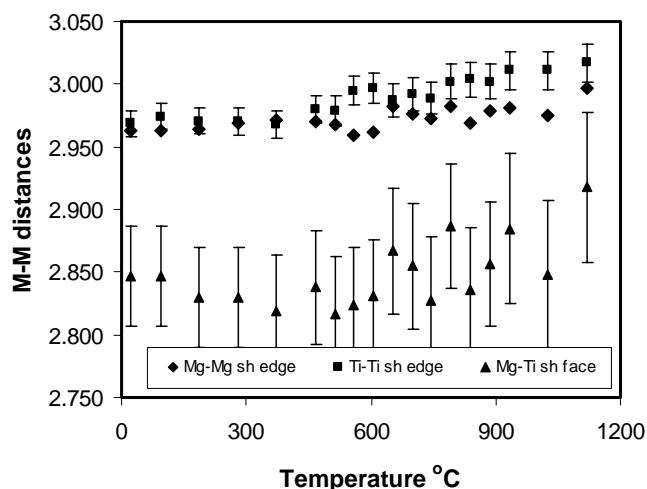


**Fig. (8).** Variation of Mg-Mg and Ti-Ti distances with temperature for geikielite (error bars are  $\pm 1\sigma$ ) across shared edges between like octahedra linked in the  $xy$  plane and for Mg-Ti distances across the shared face between  $\text{MgO}_6$  and  $\text{TiO}_6$  octahedra.

The thermal trends reported for geikielite can be compared with those reported for ilmenite [9] and show some significant differences. The best defined discrepancy is that the thermal expansion coefficient ( $\alpha$ ) for geikielite along  $a$  is smaller than that along  $c$  whereas for ilmenite  $\alpha_a > \alpha_c$ . This seems mainly related to the differences between Mg-Mg and

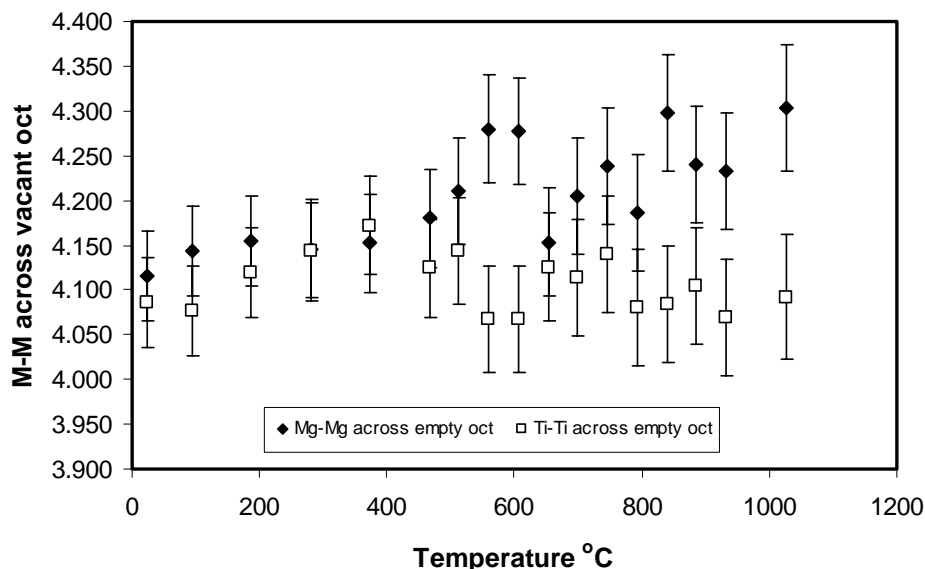


**Fig. (9).** Variation of Mg-Mg and Ti-Ti distances with temperature for geikielite along the  $c$  axis (error bars are  $\pm 1\sigma$ ) across the vacant octahedra.

Fe-Fe distances in geikielite and ilmenite respectively; the Mg-Mg distance across the empty octahedron shows a substantial expansion along  $c$  with increasing temperature in geikielite, while the equivalent Fe-Fe distance in ilmenite is reported to contract [9]. While other differences occur within the linked octahedral layers in the  $xy$  plane, these appear to be essentially second-order effects which lead to differences in the distortion parameters of the  $\text{MgO}_6$  and  $\text{TiO}_6$  polyhedra in geikielite compared to those of  $\text{FeO}_6$  and  $\text{TiO}_6$  in ilmenite.

## 5. CONCLUSIONS

- (i)  $\text{MgTiO}_3$  belongs to the space group R-3 at all temperatures which requires Mg and Ti atoms to be fully ordered confirming the earlier high-temperature Raman spectroscopy study [4].
- (ii) At all temperatures the volume of the  $\text{MgO}$  octahedron in  $\text{MgTiO}_3$  is about 20% larger than that of  $\text{TiO}_2$ .
- (iii) In  $\text{MgTiO}_3$  the Ti-O1 (shared face) bond length is much larger than the Ti-O7 (unshared face) bond length and both show small expansions with increasing temperature with the shorter bond showing the larger expansion. This is opposite to the deductions for the Ti-O octahedron in  $\text{MgTiO}_3$  based on Raman data [5] and our data are in line with the relative expansions of Mg-O and Si-O or Ge-O in analogue phases [5].
- (iv) For both octahedral species in  $\text{MgTiO}_3$  O-O edges adjacent to octahedral vacancies ('unshared edges') expand with increasing temperature while other O-O edges show either smaller increases, no change, or even small decreases. It appears that the more complicated inter-octahedral linkages lead to more restricted thermal expansion effects.
- (v) In  $\text{TiO}_2$  the length of the  $\text{O}_{1a}\text{-O}_{1a}$  bond shared between adjacent  $\text{TiO}_2$  octahedra linked along the  $c$  axis decreases with increasing temperature and the equivalent (shared)  $\text{O}_{1a}\text{-Ti-O}_{1a}$  angle also decreases. Such changes could be due to increased repulsion between adjacent Ti atoms along  $c$  as thermal motion increases [15]. Such a

relationship is also matched by the thermal expansion along *c* being larger than that perpendicular to *c*.

- (vi) The TiO<sub>2</sub> octahedron in rutile is significantly less distorted than that in geikielite (bond angle variance in rutile is ~50% of that in geikielite) which can be related to the larger number of shared edges in geikielite (three shared edges and one shared face) compared to rutile (two shared edges).

## REFERENCES

- [1] Lennie, A.R.; Knight, K.S.; Henderson, C.M.B. Cation ordering in MgTi<sub>2</sub>O<sub>5</sub> (karrooite); probing temperature dependent effects of neutrons. *Am. Mineral.*, **2007**, *92*, 1165-1180.
- [2] Cressey, G. Geikielite and perovskite in serpentine-marble from Balistan, Northern Areas (Kashmir), Pakistan. *Mineral. Mag.*, **1986**, *50*, 345-349.
- [3] Huang, C.-L.; Pan, C.-L. Structure and electrical properties of MgTiO<sub>3</sub> thin films deposited by rf magnetron sputtering. *J. Vac. Sci. Technol. A*, **2004**, *22*, 2440-2445.
- [4] Reynard, B.; Guyot, F. High-temperature properties of geikielite (MgTiO<sub>3</sub>-ilmenite) from high-temperature high-pressure Raman spectroscopy – some implications for MgSiO<sub>3</sub>-ilmenite. *Phys. Chem. Mineral.*, **1994**, *21*, 441-450.
- [5] Okada, T.; Narita, T.; Nagai, T.; Yamanaka, T. Comparative Raman spectroscopic study on ilmenite-type MgSiO<sub>3</sub> (akimotoite), MgGeO<sub>3</sub>, and MgTiO<sub>3</sub> (geikielite) at high temperatures and high pressures. *Am. Mineral.*, **2008**, *93*, 39-47.
- [6] Yamanaka, T.; Komatsu, Y.; Sugahara, M.; Nagai, T. Structure change of MgSiO<sub>3</sub>, MgGeO<sub>3</sub>, and MgTiO<sub>3</sub> ilmenites under compression. *Am. Mineral.*, **2005**, *90*, 1301-1307.
- [7] Baur, W.H. Über die Verfeinerung der Kristallstrukturbestimmung einiger Vertreter des Rutiltyps: TiO<sub>2</sub>, SnO<sub>2</sub>, GeO<sub>2</sub> und MgF<sub>2</sub>. *Acta Crystallogr.*, **1956**, *9*, 515-520.
- [8] Wechsler, B.A.; Von Dreele, R.B. Structure refinements of Mg<sub>2</sub>TiO<sub>4</sub>, MgTiO<sub>3</sub> and MgTi<sub>2</sub>O<sub>5</sub> by time-of-flight neutron powder diffraction. *Acta Crystallogr.*, **1989**, *B45*, 542-549.
- [9] Wechsler, B.A.; Prewitt, C.T. Crystal structure of ilmenite (FeTiO<sub>3</sub>) at high temperature and high pressure. *Am. Mineral.*, **1984**, *69*, 176-185.
- [10] Larson, J.C.; Von Dreele, R.B. General structure analysis system (GSAS). Los Alamos National Laboratory Report LAUR, **1994**, 86-748.
- [11] Balic Zunic, T.; Vickovic, I. IVTON – program for the calculation of geometrical aspects of crystal structures and some crystal chemical application. *J. Appl. Crystallogr.*, **1996**, *29*, 305-306.
- [12] Robinson, K.; Gibbs, G.V.; Ribbe, P.H. Quadratic elongation: a quantitative measure of distortion in coordination polyhedra. *Science*, **1971**, *172*, 567-570.
- [13] Meagher, E.P.; Lager, G.A. Polyhedral thermal expansion in the TiO<sub>2</sub> polymorphs: refinement of the crystal structures of rutile and brookite at high temperature. *Can. Mineral.*, **1979**, *17*, 77-85.
- [14] Burdett, J.K.; Hughbanks, T.; Miller, G.J.; Richardson, J.W.; Jr.; Smith, J.V. Structural electronic relationships in inorganic solids - powder neutron-diffraction studies of the rutile and anatase polymorphs of titanium dioxide at 15 and 295K. *J. Am. Chem. Soc.*, **1987**, *109*, 3639-3646.
- [15] Sugiyama, K.; Takéuchi, Y. The crystal structure of rutile as a function of temperature up to 1600°C. *Zeits. Krist.*, **1991**, *194*, 305-313.
- [16] Seki, H.; Ishizawa, N.; Mizutani, N.; Kato, M. High temperature structure of the rutile type oxides, TiO<sub>2</sub> and SnO<sub>2</sub>. *J. Ceram. Soc. Japan*, **1984**, *92*, 219-223.
- [17] Abrahams, S.C.; Bernstein, J.L. Rutile: normal probability plot analysis and accurate measurement of crystal structure. *J. Chem. Phys.*, **1971**, *55*, 3206-3211.
- [18] Rao, K.V.K.; Naidu, S.V.N.; Iyengar, L. Thermal expansion of rutile and anatase. *J. Am. Ceram. Soc.*, **1970**, *53*, 124-126.
- [19] Merz, K.M.; Brown, W.R.; Kirchner, H.P. Thermal-expansion anisotropy of oxide solid solutions. *J. Am. Ceram. Soc.*, **1962**, *45*, 531-536.
- [20] Taylor, D. Thermal expansion data: II Binary oxides with the fluorite and rutile structures, MO<sub>2</sub>, and the antifluorite structure, M<sub>2</sub>O. *J. Br. Ceram. Soc.*, **1984**, *83*, 32-37.
- [21] Liferovich, R.P.; Mitchell, R.H. The pyrophanite-geikielite solid-solution series: crystal structures of the Mn<sub>1-x</sub>Mg<sub>x</sub>TiO<sub>3</sub> series (0<x<0.7). *Can. Mineral.*, **2006**, *44*, 1099-1107.
- [22] Liferovich, R.P.; Mitchell, R.H. Geikielite-ecandrewsite solid-solutions: synthesis and crystal structures of the Mg<sub>1-x</sub>Zn<sub>x</sub>TiO<sub>3</sub> series (0<x<0.8) series. *Acta Crystallogr.*, **2004**, *B60*, 496-501.
- [23] Liferovich, R.P.; Mitchell, R.H. Rhombohedral ilmenite group nickel titanates with Zn, Mg, and Mn: synthesis and crystal structures. *Phys. Chem. Mineral.*, **2005**, *32*, 442-449.

Received: December 12, 2008

Revised: February 4, 2009

Accepted: March 3, 2009

© Henderson *et al.*; Licensee Bentham Open.

This is an open access article licensed under the terms of the Creative Commons Attribution Non-Commercial License (<http://creativecommons.org/licenses/by-nc/3.0/>) which permits unrestricted, non-commercial use, distribution and reproduction in any medium, provided the work is properly cited.